Brain Network Allostasis after Chronic Alcohol Drinking Is Characterized by Functional Dedifferentiation and Narrowing

Perez-Ramirez, Ursula

2022-05-25

Perez-Ramirez , U , Lopez-Madrona , V J , Perez-Segura , A , Pallares , V , Moreno , A , Ciccocioppo , R , Hyytiä , P , Sommer , W H , Moratal , D & Canals , S 2022 , ' Brain Network Allostasis after Chronic Alcohol Drinking Is Characterized by Functional Dedifferentiation and Narrowing ' , Journal of Neuroscience , vol. 42 , no. 21 , pp. 4401-4413 . https://doi.org/10.1523/JNEUROSCI.0389-21.2022

http://hdl.handle.net/10138/351154
https://doi.org/10.1523/JNEUROSCI.0389-21.2022

Neurobiology of Disease

Brain Network Allostasis after Chronic Alcohol Drinking Is Characterized by Functional Dedifferentiation and Narrowing

Úrsula Pérez-Ramírez,[1] Víctor J. López-Madrona,[2] Andrés Pérez-Segura,[2] Vicente Pallarés,[2] Andrea Moreno,[2] Roberto Ciccocioppo,[3] Petri Hyytiä,[4] Wolfgang H. Sommer,[5] David Moratal,[1] and Santiago Canals[2]

[1]Center for Biomaterials and Tissue Engineering, Universitat Politècnica de València, E-46022 Valencia, Spain, [2]Instituto de Neurociencias, Consejo Superior de Investigaciones Científicas, Universidad Miguel Hernández, 03550 Sant Joan d'Alacant, Spain, [3]School of Pharmacy, University of Camerino, 62032 Camerino, Italy, [4]Department of Pharmacology, Faculty of Medicine, University of Helsinki, 00014 Helsinki, Finland, and [5]Institute of Psychopharmacology, Central Institute of Mental Health, Medical Faculty Mannheim, University of Heidelberg, 68159 Mannheim, Germany

Alcohol use disorder (AUD) causes complex alterations in the brain that are poorly understood. The heterogeneity of drinking patterns and the high incidence of comorbid factors compromise mechanistic investigations in AUD patients. Here we used male Marchigian Sardinian alcohol-preferring (msP) rats, a well established animal model of chronic alcohol drinking, and a combination of longitudinal resting-state fMRI and manganese-enhanced MRI to provide objective measurements of brain connectivity and activity, respectively. We found that 1 month of chronic alcohol drinking changed the correlation between resting-state networks. The change was not homogeneous, resulting in the reorganization of pairwise interactions and a shift in the equilibrium of functional connections. We identified two fundamentally different forms of network reorganization. First is functional dedifferentiation, which is defined as a regional increase in neuronal activity and overall correlation, with a concomitant decrease in preferential connectivity between specific networks. Through this mechanism, occipital cortical areas lost their specific interaction with sensory-insular cortex, striatal, and sensorimotor networks. Second is functional narrowing, which is defined as an increase in neuronal activity and preferential connectivity between specific brain networks. Functional narrowing strengthened the interaction between striatal and prefrontocortical networks, involving the anterior insular, cingulate, orbitofrontal, prelimbic, and infralimbic cortices. Importantly, these two types of alterations persisted after alcohol discontinuation, suggesting that dedifferentiation and functional narrowing rendered persistent network states. Our results support the idea that chronic alcohol drinking, albeit at moderate intoxicating levels, induces an allostatic change in the brain functional connectivity that propagates into early abstinence.

Key words: **alcohol; allostasis; AUD; fMRI; MEMRI; network**

Received Feb. 21, 2021; revised Mar. 25, 2022; accepted Mar. 30, 2022.

Author contributions: Ú.P.-R., V.J.L.-M., V.P., R.C., P.H., W.H.S., D.M., and S.C. designed research; Ú.P.-R., A.M. and P.H. performed research; A.M. and R.C. contributed unpublished reagents/analytic tools; Ú.P.-R., V.J.L.-M., A.P.-S., V.P., D.M., and S.C. analyzed data; Ú.P.-R., V.J.L.-M., D.M., and S.C. wrote the paper.

This research was supported by funding from the European Union Horizon 2020 research and innovation program under Grant 668863 (SyBil-AA); the ERA-Net NEURON framework with grants given to the project "Translational Neuroimaging in Alcoholism" (TRANSALC) by the Academy of Finland (Grant TRANSALC 01EW1112), the Bundesministerium für Bildung und Forschung (Grant FKZ01EW1112), and the Spanish Ministerio de Ciencia e Innovación (Grant PIM2010ERN-00679). S.C. and D.M. were funded by the Spanish Ministerio de Economía y Competitividad (MINECO) cofinanced by the European Regional Development Fund (ERDF) under Grants BFU2015-64380-C2-1-R and BFU2015-64380-C2-2-R, and the Generalitat Valenciana Government through the Prometeo Program (Grant PROMETEO/2019/015). S.C. was further supported by the Spanish Agency of Research (AEI) and ERDF under Grant PGC2018-101055-B-I00 and the Spanish Ministerio de Sanidad, Servicios Sociales e Igualdad (Grant 2017I065). Ú.P.-R. was supported by Grant FPU13/03537 and research stay internship EST15/00516 from the Spanish Ministerio de Educación, Cultura y Deporte (MECD). Further funding was obtained from the Spanish State Research Agency through the Severo Ochoa Program for Centres of Excellence in R&D (Grant SEV- 2017-0723). W.H.S. was further supported by the Deutsche Forschungsgemeinschaft (Center Grant TRR265-B08). We thank Eugene Duff and Stephen Smith for comments on a previous version of this manuscript. We also thank Begoña Fernández for technical assistance.

V.J. López-Madrona's present address: Aix Marseille University, INSERM, INS, Institut de Neurosciences des Systèmes, 13005 Marseille, France.

A. Moreno's present address: Danish Research Institute of Translational Neuroscience (DANDRITE), Aarhus University, 8000 Aarhus, Denmark.

The authors declare no competing financial interests.

Correspondence should be addressed to David Moratal at dmoratal@eln.upv.es or Santiago Canals at scanals@umh.es.

https://doi.org/10.1523/JNEUROSCI.0389-21.2022

Significance Statement

Excessive consumption of alcohol is positioned among the top five risk factors for disease and disability. Despite this priority, the transformations that the nervous system undergoes from an alcohol-naive state to a pathologic alcohol drinking are not well understood. In our study, we use an animal model with proven translational validity to study this transformation longitudinally. The results show that shortly after chronic alcohol consumption there is an increase in redundant activity shared by brain structures, and the specific communication shrinks to a set of pathways. This functional dedifferentiation and narrowing are not reversed immediately after alcohol withdrawal but persist during early abstinence. We causally link chronic alcohol drinking with an early and abstinence-persistent retuning of the functional equilibrium of the brain.

Introduction

Excessive consumption of alcohol is positioned among the top five risk factors for disease and disability worldwide and alcohol use disorders (AUDs) have a prevalence of 5.1% in a population aged ≥15 years (World Health Organization, 2018). These alarming numbers worsen in the light of recent studies indicating that there is no safe level of alcohol consumption (Topiwala et al., 2017). Despite this priority and a strongly growing body of literature, we still have a poor understanding of the brain mechanisms underlying this aberrant behavior, especially of those alcohol-induced alterations that are accessible to objective measurements and that may comprise early warning signs for an ongoing disease process (Heilig et al., 2019).

Functional magnetic resonance imaging (fMRI), in particular the measurement of spontaneous or intrinsic neural activity at rest [resting-state fMRI (rs-fMRI)], can be used for examining brain-wide networks (Fox and Raichle, 2007; Cole et al., 2010). With this technique, networks can be generated with nodes defined either by a priori criteria, anatomic or functional, or by data-driven criteria, based on the signal dynamics in the individual imaged points or voxels. In the second modality, the nodes, also called resting-state networks (RSNs), are composed by brain regions that share activity patterns, and one brain region can contribute to more than one RSN. The links connecting pairs of RSNs in a brain-wide network are often defined as the correlation strength between the activity time courses in the nodes. Correlation analysis of blood oxygenation level-dependent (BOLD) signals from rs-fMRIs of AUD patients has shown diverse alteration in various RSNs (Chanraud et al., 2011; Weiland et al., 2014; Müller-Oehring et al., 2015; Dupuy and Chanraud, 2016; Zhu et al., 2016, 2017; Kohno et al., 2017; Vergara et al., 2017). While these studies provide a valuable account of the functional alterations associated with persistent alcohol consumption, establishing causality to the pathophysiology of AUD is challenging. Clinical studies inherently contain various potential confounds such as different patterns of abuse, often including multiple substances, heterogeneity in disease phenotype, somatic and psychiatric comorbidity, smoking, nutrition, and socioeconomic factors, to name a few. Furthermore, the neural alterations occurring during the transition from an alcohol-naive state to a pathologic drinking state are difficult to investigate longitudinally in human subjects.

In contrast, MRIs in laboratory animals provide the tight experimental control necessary for establishing causality. The high translational utility of animal AUD models has been recently demonstrated, using structural and functional MRI, in the identification of a novel pathologic mechanism during the early weeks of abstinence after high voluntary alcohol consumption (De Santis et al., 2019, 2020; Scuppa et al., 2020). However, when investigating functional connectivity (FC) with MRI in experimental rodents, the use of anesthesia needs to be considered (Moreno et al., 2013; Pan et al., 2015). While experiments in rodents (Paasonen et al., 2018) and primates (Vincent et al., 2007) show a comparable organization of resting-state connections in awake versus anesthetized conditions, which mostly recapitulate the underlying known structural connectivity (Barttfeld et al., 2015; Díaz-Parra et al., 2017), complementary measurements of brain activity in awake conditions are desirable. Awake fMRI studies in rodents have been developed (Zhang et al., 2010; Stenroos et al., 2018) but involve habituation periods of intense stress, which will unavoidably interfere with animal models in which the stress is an important factor, as is the case in AUD (Ciccocioppo et al., 2006; Ciccocioppo, 2013).

Other functional imaging modalities, such as manganese-enhanced MRI (MEMRI), permit recordings of brain-wide network activations produced during awake and behaving conditions. The paramagnetic ion manganese (Mn^{2+}) permeates cells through voltage-gated calcium channels and accumulates in depolarized neurons. Since Mn^{2+} clearance is slow, the pattern of activity-dependent Mn^{2+} accumulation produced in awake conditions can then be measured as increased signal intensity in T1-weighted images (Silva et al., 2004; Eschenko et al., 2010a). This technique has been successfully used to identifying neural circuits associated with specific behaviors (Eschenko et al., 2010a; Gildish et al., 2012; Bangasser et al., 2013; McGuire et al., 2013; Laine et al., 2017; Yang and Li, 2020), including cocaine addiction (Cannella et al., 2020) and excessive alcohol drinking in rats (Dudek et al., 2015, 2016; Pallarés et al., 2021).

Here we used a multimodal MRI approach combining anesthetized BOLD-contrast fMRI and awake MEMRI. We thus complemented functional connectivity with regional neuronal activity analysis to provide new insight in the early remodeling of brain networks initiated by chronic alcohol drinking. We used the Marchigian Sardinian alcohol-preferring (msP) rat line (Ciccocioppo, 2013), a well established model that has demonstrated strong translational value (De Santis et al., 2019, 2020). This rat line consumes pharmacologically relevant blood alcohol levels inducing reward, antidepressant and anxiolytic actions (Ciccocioppo et al., 2006; Borruto et al., 2021), matching some of the characteristic alcohol effects in AUD patients.

Following 1 month of voluntary alcohol drinking, we identified widespread changes in functional connectivity patterns and increased neuronal activations in prefrontocortical and striatal regions. Interestingly, two fundamentally different forms of network reorganization emerged according to the pattern of connectivity induced by alcohol drinking. These changes defined a new alcohol-driven equilibrium state that does not return to baseline on alcohol withdrawal but propagates into early abstinence.

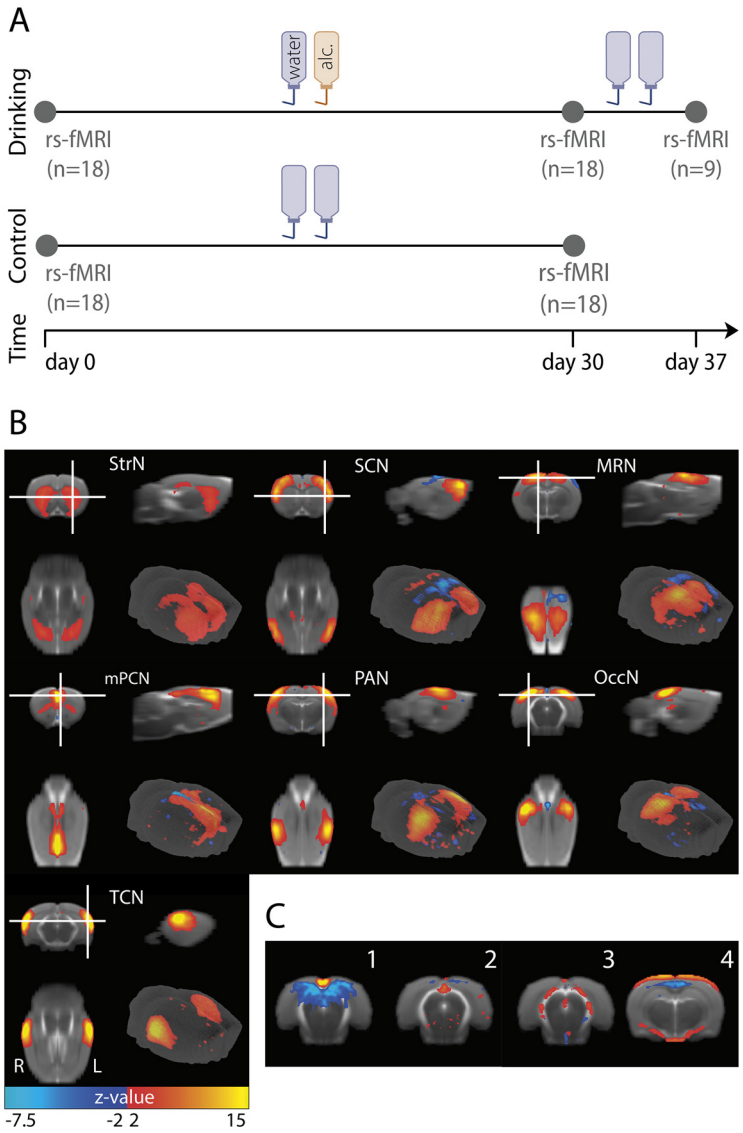

Figure 1. Experimental rs-fMRI design and RSNs obtained with group-PICA. ***A***, Schematic representation of the rs-fMRI experiment. ***B***, RSNs obtained considering naive and alcohol conditions. From bottom left, clockwise: axial, coronal, sagittal, and three-dimensional views of StrN, SCN, MRN, mPCN, PAN, OccN, and TCN. ***C***, Four (1–4) discarded ICs produced by group-PICA and corresponding to blood vessels or movement artifacts.

Materials and Methods

Animals and experimental design. A total of 72 male msP rats (age, 4 months; weight, 370–480 g) were imported from the breeding facility at University of Camerino, Italy (Ciccocioppo et al., 2006; Ciccocioppo, 2013). Two cohorts ($n = 36$ rats) were used for longitudinal fMRI studies, and another two cohorts ($n = 36$ rats) were used for MEMRI. Part of the MEMRI data were used in a recent report comparing two alcohol-preferring rat strains (Cohort 3 below; Pallarés et al., 2021). For the experiments, the rats were individually housed in transparent polycarbonate cages with bedding, a wood stick, and nesting material, with *ad libitum* access to food and water, regulated temperature (21 ± 1°C), and relative humidity (55 ± 10%), and on a regular 12 h light/dark cycle (lights on at 8:00 A.M.). All experiments were approved by the Animal Care and Use Committee of our institution (Consejo Superior de Investigaciones Científicas) and comply with the Spanish (law 32/2007) and European regulations (EU directive 86/609, EU decree 2001–486, and EU recommendation 2007/526/EC).

Two rs-fMRI longitudinal studies were conducted. Animals of Cohort 1 ($n = 18$) had free access to alcohol in a two-bottle free-choice paradigm (two 250 ml drinking bottles: one filled with water, the other containing 10% ethanol in water, changed and measured twice per week) and were imaged at the following three time points: (1) before alcohol access [naive condition, time point 1 (TP1)]; (2) after 30 d of alcohol drinking (alcohol condition, TP2); and (3) after 1 week without alcohol access (abstinent condition, TP3). For the last scan, only nine randomly selected animals were used. Cohort 2 ($n = 18$) was imaged twice in the alcohol-naive condition with a 30 d interval (TP1 and TP2) and was used as a control to account for any age-related differences in brain resting state FC (Fig. 1*A*).

Cohort 3 for the MEMRI experiment was assessed in a cross-sectional design, with the alcohol-drinking group ($n = 14$) having access to water and alcohol, as described above, and the control group ($n = 14$) having access only to water during the same 30 d (see Fig. 7*A*). In this cohort, $MnCl_2$ was administered using an osmotic minipump (model 2001, ALZET) delivering 200 µl of $MnCl_2$ (1 µl/h) during a 7 d infusion period. $MnCl_2$ was prepared as an isotonic solution dissolved in Tris-buffered saline, pH 7.4. The total dose of infused $MnCl_2$ was 80 mg/kg. Before the surgery, the pumps were primed overnight in a 37°C saline solution. The pumps were implanted subcutaneously on the dorsum, slightly caudal to the scapulae. Animals were imaged immediately following the 7 d $MnCl_2$ infusion.

In Cohort 4, we investigated the influence of the manganese administration time window on the obtained activity maps. In the previous MEMRI experiment, the obtained activation maps represented the integrated manganese accumulation over the last drinking week. However, in the rs-fMRI experiments, we measured functional connectivity on the last day of alcohol drinking. To compare both imaging time windows, we performed one additional MEMRI experiment with an acute injection of 80 mg/kg, i.p., $MnCl_2$ (in Tris-buffered saline), pH 7.4, before both the alcohol-drinking phase (TP1) and the final 24 h drinking session (TP2), and then imaged manganese accumulation 24 h later. In this within-subjects design ($n = 8$), functional MEMRI maps represent brain activity on the last day of alcohol drinking (see Fig. 6*A*).

MRI acquisition protocol. The experiments were conducted in a horizontal 7 tesla MRI scanner containing a 30-cm-diameter bore (Biospec 70/30v, Bruker Medical) and a 675 mT/m actively shielded gradient coil (model BGA 12-S, Bruker) of 11.4 cm inner diameter. To achieve the highest possible signal-to-noise ratio (SNR), a 1H rat brain receive-only phase array coil with integrated combiner and preamplifier, no tune/no match was used together with the actively detuned transmit-only resonator (BrukerBioSpin MRI). MRI images were acquired and minimally preprocessed with a Hewlett-Packard console running Paravision 5.1 software (Bruker Medical) on a Linux platform. The msP rats were placed in an MRI-compatible stereotaxic device with adjustable ear bars and bite bars on the magnet bed. To maintain the vascular reactivity triggered by neuronal activation, the temperature of the rats was preserved (37 ± 0.5°C) using a water blanket connected to a temperature-regulated water bath (SAHARA S5P Heated Bath Circulators, Thermo Fisher Scientific). Furthermore, vital constants were monitored (MouseOx, Starr Life Sciences) to make sure that the following optimal values were fulfilled: heart rate (300 ± 50 beats/min), oxygen saturation (>95%), and breathing rate (90 ± 10 breaths/min; Pacheco-Torres et al., 2018; Pérez-Cervera et al., 2018).

rs-fMRI data acquisition. The msP rats were anesthetized with 1% isoflurane in oxygen (0.8–1 L/min). rs-fMRI acquisition was performed using a gradient echo-EPI sequence with the following parameters: field of view (FOV) = 25 × 25 mm; slice thickness = 1 mm; 15 coronal slices; five 3 min runs; matrix size = 96 × 96 voxels; flip angle = 60°; echo time (TE) = 15 ms; and repetition time (TR) = 2000 ms. To facilitate the registration of these functional images to a standard space, we also collected anatomic T2-weighted MRI images, using rapid acquisition relaxation enhanced sequence (RARE) and applying the following acquisition parameters: FOV = 25 × 25 mm; slice thickness = 1 mm; 15 coronal slices; matrix size = 192 × 192 voxels; RARE factor = 8; effective TE = 56 ms; and TR = 2000 ms.

MEMRI data acquisition. T1-weighted images were acquired on the anesthetized rats (1% isoflurane in oxygen, 0.8–1 L/min) using a multislice multiecho pulse sequence (TR = 300 ms; TE = 14 ms; averages = 8; FOV = 32 × 32 mm; and 9 horizontal slices of 0.5 mm thickness with matrix size = 256 × 256 voxels, resulting in $0.125 \times 0.125 \times 0.5$ mm^3 voxel resolution).

rs-fMRI image preprocessing. rs-fMRI data were preprocessed within runs using FSL 5.07 tools (Oxford Center for Functional MRI of the Brain, Oxford, UK; Smith et al., 2004; Jenkinson et al., 2012) and MATLAB 2014a (MathWorks). First, the Bruker images were converted to NIfTI (Neuroimaging Informatics Technology Initiative) data format, and the voxel resolution was scaled up by 10 to mimic human brain size and apply correct spatial transformations (Kalthoff et al., 2011; Pan et al., 2015). Afterward, motion correction was applied with respect to the middle volume (Jenkinson et al., 2002) and the brain was segmented (Smith, 2002). Next, the transformation matrix to register the functional images to a rat brain T2-weighted MRI template (Schwarz et al., 2006) was calculated as the concatenation of two matrices: (1) rigid matrix to coregister the functional images onto the anatomic image; and (2) affine matrix to register the anatomic images to the standard template. The next step was noise reduction, including a 4 mm full-width at half-maximum (FWHM) Gaussian smoothing (Smith and Brady, 1997). Subsequently, global 4D mean-based intensity normalization was applied and the variance tied to six motion parameters (rotations and translations along the three principal axes) was regressed out. This step was followed by a bandpass temporal filtering (nonlinear high-pass filter, $\sigma = 50$ s; Gaussian linear low-pass filter, $\sigma = 2$ s) to retain frequencies in the 0.01–0.1 Hz range, the frequency band with biological relevance for rodents under isoflurane anesthesia (Pan et al., 2013). Finally, the transformation matrix was applied to the functional images, which became normalized to a standard space (Schwarz et al., 2006).

Next, to obtain run-specific time series of each RSN, the following two steps were performed: group probabilistic independent component analysis (PICA) and spatial regression.

Group probabilistic independent component analysis. PICA (Beckmann et al., 2005) was applied to the data (individual runs) in naive and alcohol conditions in Cohort 1, using MELODIC (Multivariate Exploratory Linear Decomposition into Independent Components) version 3.14, part of FSL (FMRIB Software Library; Smith et al., 2004; Jenkinson et al., 2012). The aim of this data-driven approach is to find group linear-mixed, independent and non-Gaussian sources, leading to spatial maps with minimal spatial redundancy, each of them having voxels that share a unique time course (Smith et al., 2014). Before this analysis, each brain-extracted image was voxel-wise preprocessed, including demeaning and variance normalization. Then, these data were temporally concatenated across control and alcohol conditions, whitened, and projected into a 17-dimensional subspace using principal component analysis. Seventeen dimensions were the best balance between the fusion and separation of brain regions of the same RSN. The whitened observations were decomposed into sets of vectors that describe signal variation across the temporal domain (time courses), the run domain, and the spatial domain (maps) by optimizing for non-Gaussian spatial source distributions using a fixed-point iteration technique (Hyvärinen, 1997). Then, the estimated component maps were divided by the SD of the residual noise and threshold to place equal loss on false positives and false negatives, by fitting a mixture model to the histogram of intensity values (Beckmann and Smith, 2004). Group-PICA parceled the functional data into 17 independent components (ICs)—spatial maps and time courses—some reflecting spatial artifacts, blood vessels, or CSF (Fig. 1*C*), and others corresponding to well characterized RSNs (Fig. 1*B*; Becerra et al., 2011).

Spatial regression. To obtain run-specific time courses for the ICs identified by group-PICA, we used the first step of dual-regression (i.e., spatial regression). The whole set of group-PICA spatial maps was spatially regressed onto the rs-fMRI data, obtaining run-specific β-coefficients that characterize the temporal dynamics for each spatial map—time courses for each group-PICA map—and condition (Beckmann et al., 2009; Smith et al., 2014).

Direct and indirect rs-FC. To investigate the interactions between RSN in the brain-wide network, we followed an approach based on multiple multivariate linear regressions (mlrs), combining full and partial models (López-Madrona et al., 2020). For each RSN or node ($Node_d$), we have defined an mlr, where the target node ($Node_d$) is defined by a linear combination of the other nodes, or factors, plus a residual, as follows:

$$Node_d = \beta_0 + \beta_1 Node_1 + \beta_2 Node_2 + \beta_3 Node_3 + \ldots + \varepsilon,$$

where β_0 is a constant value and ε is the residuals.

This model gives the total variance of $Node_d$ that can be explained by all the other nodes (variance of $\beta_0 + \beta_1 Node_1 + \beta_2 Node_2 + \ldots + \beta_n Node_n$) and the unexplained variance (variance of ε). We call the total explained variance var_{full}.

Using different subsets of this model, it is possible to identify the variance that is explained by each factor or combination of them. For example, if only one factor is included in the model:

$$Node_d = \beta_0 + \beta_1 Node_1 + \varepsilon.$$

We would obtain the total variance that can be explained by $Node_1$, independent of the contributions of other nodes. It can be compared with the full correlation between $Node_d$ and $Node_1$. We call this variance var_{1full}.

To obtain the variance that is explained solely by $Node_1$, which cannot be explained by any other factor, we remove Node1 from the full mlr, as follows:

$$Node_d = \beta_0 + \beta_2 Node_2 + \beta_3 Node_3 + \ldots + \varepsilon.$$

The difference between the var_{full}, minus the variance explained with all factors except $Node_1$, would indicate the specific contribution of $Node_1$ to $Node_d$. We call this variance var_{1par}. This can be compared with the partial correlation between $Node_d$ and $Node_1$.

The next question would be, in case that var_{1par} is lower, which of the other nodes are explaining the same variance of $Node_1$? We can address the variance shared by two nodes with a submodel including them. Continuing with the example, if we are interested in the variance of $Node_d$ that is explained by $Node_1$ but that can be also explained by $Node_2$, the first step is to compute an mlr with both factors, as follows:

$$Node_d = \beta_0 + \beta_1 Node_1 + \beta_2 Node_2 + \varepsilon.$$

We call var_{12full} the variance that is explained by $Node_1$ and $Node_2$. Then, we compute the submodel including only the second factor, obtaining var_{2full}. In a similar manner as before, the variance that is explained by $Node_1$ that cannot be accounted by $Node_2$ is obtained as the difference between var_{12full} minus var_{2full}. We call this variance var_{1par2}. This value should be equal or higher than var_{1par}, and lower or equal than var_{1full}. Furthermore, the difference between var_{1full} minus var_{1par2} would be the proportion of variance explained by $Node_1$, which is also explained by $Node_2$. In other words, this can be interpreted as the indirect information between $Node_d$ and $Node_1$, which is mediated by $Node_2$. Note that this indirect pathway may also be shared by other nodes in the network. However, we did not further partialize the model as it may result in negligible connectivity values.

We first used Cohorts 1 and 2 to assess whether changes in RSN connectivity were solely driven by alcohol drinking or had an age-related contribution. To this end, we first computed the difference in the global connectivity (average of all full connectivity values) between the two time points (1 month interval) in each cohort, and then compared the difference using a two-tailed Wilcoxon rank-sum test. We then tested in Cohort 1 the longitudinal transformations induced by alcohol drinking. Finally, using Cohort 1, we further tested whether 1 week of abstinence after 1 month of alcohol exposure induced any further alteration or homeostatic recovery of connectivity. To compare network interactions between conditions, we first concatenated the time series per subject and group, and computed the regressions in the concatenated data. After that, we averaged the results across subjects and computed the difference between conditions. For the statistical analysis, we followed a surrogate approach. We computed 1000 surrogates by randomly switching the runs of each subject between experimental conditions. The result of each surrogate in each condition was given by the average across subjects. Finally, we computed the difference between both conditions. These surrogate distributions can be approximated to normal. The p-values associated with each result were determined as the cumulative surrogate distribution evaluated at that point (i.e., difference between conditions). We corrected for multiple comparisons by multiplying the resultant p-values by the number of links analyzed (21 pairs).

Estimating rs-FC with regularized partial correlation. We further used a more restrictive method to measure partial correlation between RSNs, which is especially suited for time series with a low number of samples, as in the case of fMRI. We used FSLNets toolbox version 0.6, part of FSL. After demeaning each time course, the time courses from the discarded ICs were regressed out of the time courses of the RSNs (Griffanti et al., 2014), and the rest of the analysis was focused only on the cleaned time courses of the RSNs. We next computed the L2-regularized partial correlation (ridge regression with $\rho = 0.01$; Smith et al., 2011, 2015) between each pair of time courses, for each run, with the goal of solely focusing on direct network connections. Then, the partial correlation values were converted into Fisher's z-transformed values considering the temporal smoothness of the data, and the network matrices were averaged across five runs to obtain one network matrix per subject.

For the statistical analysis, the BOLD signal at each voxel was modeled with the general linear model (Friston et al., 1994), applied using permutation-based nonparametric testing, correcting for multiple comparisons. The p-values were family wise error rate corrected for multiple comparisons and contrasts (Winkler et al., 2014, 2016) in an analysis subjected to 5000 permutations. The difference in L2-regularized partial correlation values of each pair of networks between the two time points (1 month interval) were calculated for the drinking (Cohort 1) and control (Cohort 2) groups, and were compared using a two-way ANOVA followed by a Bonferroni's multiple-comparison test. In addition, longitudinal comparisons between naive and alcohol-exposed states were performed with a paired t test in Cohort 1. Finally, the effect of abstinence was further tested in Cohort 1 with a paired t test between-network rs-FC of the nine msP rats in alcohol-exposed versus abstinence conditions.

MEMRI image preprocessing. All images were preprocessed with custom-developed MATLAB functions (version R2014a; MathWorks) and FSL 5.07 tools (Oxford Center for Functional MRI of the Brain; Smith et al., 2004; Jenkinson et al., 2012). First, the MEMRI images were converted to NIfTI format, scaled up by a factor of 10 and brain extracted (Smith, 2002). Then, these T1-weighted images were coregistered and further registered to a stereotaxic rat brain MRI template (Schwarz et al., 2006) by a 12-parameter affine transformation (Jenkinson et al., 2002). This template is coregistered to a digitized atlas (Paxinos and Watson, 2007), which enables atlas-based generation of region of interest (ROI) masks for detailed anatomic analysis. The resulting images were smoothed to improve SNR using a Gaussian kernel with $4 \times 4 \times 4$ mm^3 FWHM. Afterward, the percentage of voxels that showed a statistically significant increase in signal intensity per ROI was calculated.

MEMRI data analysis. For identifying the brain regions in which activation in the alcohol-drinking group differed from that in the control group, voxel-wise independent t tests were performed in SPM8 (Wellcome Trust Center for Neuroimaging, Institute of Neurology, University College London, London, UK). An initial arbitrary significance threshold was set to $p < 0.01$ (uncorrected) for individual voxels, and then a cluster size threshold was applied to correct for multiple comparisons at $p < 0.05$. The cluster size threshold value was determined using Monte Carlo simulation. More restrictive statistical thresholds were also tested (see Results). Finally, the voxels with significant differences in activity across control and alcohol conditions were grouped into brain regions corresponding to the RSN found with fMRI, and the percentage of activated voxels within each one was calculated.

Results

Resting-state networks

During the 1 month of alcohol access (Fig. 1*A*), animals had an average alcohol consumption of 5.8 ± 1.4 g/kg/d. To assess changes in resting-state connectivity induced by this level of alcohol consumption, we first used group-PICA to define data-driven and robust components from the rs-fMRI data in the longitudinal imaging experiment (Fig. 1*B*). We found seven distinct RSNs that we named according to the dominant brain regions represented in the network. In some cases (see below), the identified networks resembled those found in humans and rodents under operational/cognitive definitions, such as the salience, the reward, or the default-mode networks. We found a striatal network (StrN), composed of the caudate putamen, nucleus accumbens (NAc), and the ventral pallidum, also invading a portion of the dorsal hippocampus (HC). The sensory-cortex network (SCN), which included mainly posterior insular cortex, primary somatosensory cortex (S1), and secondary somatosensory cortex (S2), and invaded some primary motor cortex regions, with S1 being the region with the highest IC values. The motor-retrosplenial network (MRN), formed by primary and secondary motor cortices and retrosplenial cortices, invading small portions of S1 and S2. The medial prefrontal-cingulate network (mPCN) is principally composed by the anterior cingulate cortex and the prelimbic cortex, and contributed by the infralimbic cortex, lateral orbital cortex, and the anterior insula (AI). The parietal-association network (PAN) is centered in the parietal cortex (Pa) and extends into some regions of S1 and S2. The occipital network (OccN), primarily centered on the primary visual cortex (V1) and secondary visual cortex, spreading into the HC, S1, and laterodorsal thalamic nucleus. And the temporal-cortex network (TCN), which included the temporal association cortex, primary and secondary auditory cortices, and part of V1.

Network connectivity

We first investigated FC in the brain-wide network of RSNs using multiple multivariate linear regression (see Materials and Methods), differentiating among global, specific (partialized), and indirect interactions. Global interaction after 1 month, accounting for the full relation among all pairs of RSNs (comparable to full correlation), was found to be significantly higher in alcohol-drinking compared with control (water-drinking) animals (two-tailed Wilcoxon rank-sum test, $p = 0.0031$; Fig. 2*A*). While all RSNs showed an overall increase in connectivity in the alcohol condition, the magnitude of this change was heterogeneously distributed among individual networks (Fig. 2*B*).

The heterogeneity of the effects of alcohol on RSN connectivity was even more evident at the level of individual links (Fig. 3*A*). For instance, the full connectivity of the StrN was significantly increased only with the mPCN and MRN, but not with the other networks. With these results, we speculated that the

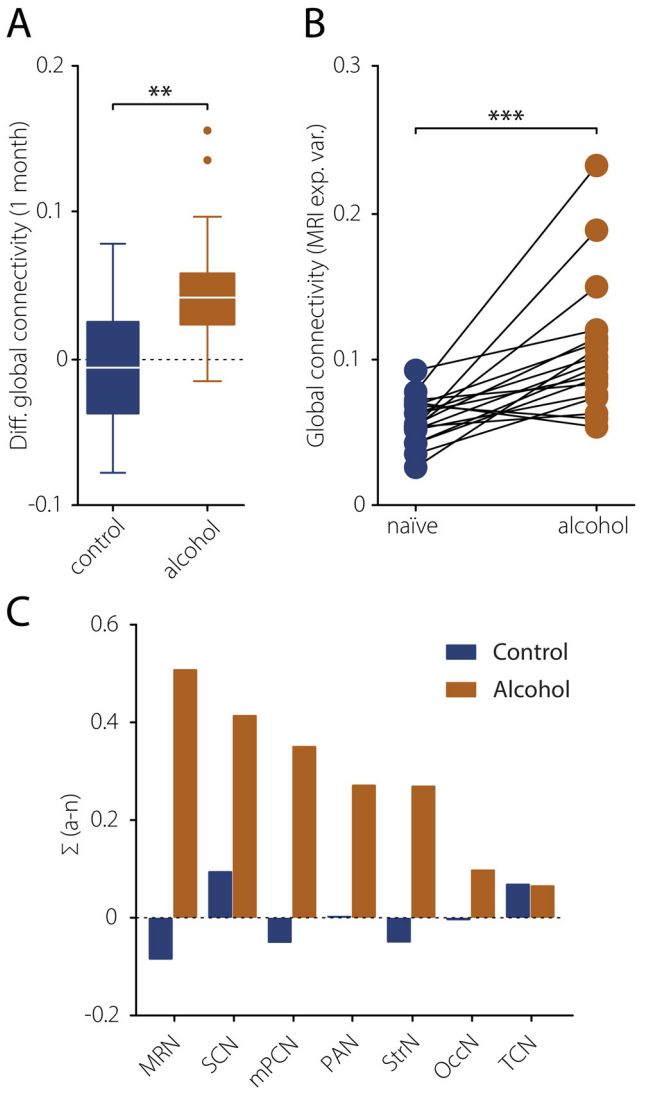

Figure 2. Global connectivity is increased by alcohol drinking. ***A***, Comparison of changes in global connectivity, measured as the average of all full connectivity values per subject, after 1 month in the alcohol-drinking versus the control group. The central mark of the box indicates the median, and the bottom and top edges of the box indicate the 25th and 75th percentiles, respectively. The whiskers extend to the most extreme data points not considered outliers, and the outliers are plotted individually as colored dots. $^{**}p < 0.01$. ***B***, The increment in link strength in alcohol versus naive conditions is heterogeneously distributed across RSNs. $^{***}p < 0.001$. ***C***, Link strength difference (alcohol – naive) was summed for all links of each node. $^{***}p < 0.001$.

specific information shared by the RSNs might have changed after chronic alcohol drinking. We therefore computed direct interactions in the network, as the partial relation between two RSNs that cannot be explained by any other RSNs (comparable to partial correlation; Fig. 3*B*). Complementarily, we also computed the information between two RSNs that is also contained in a third RSN (indirect relation; Fig. 3*C*). Interestingly, while most partial interactions were stable across conditions, we found that the balance of specific pair-wise interactions between some RSNs was dramatically changed in the alcohol group (Fig. 3*B*). Furthermore, contrary to the consistent increase in full relations, specific pair-wise interactions could increase or decrease. Significant increases were found between the StrN and mPCN ($p < 0.025$ based on surrogate measures; see Materials and Methods) and SCN-PAN ($p < 0.025$), and decreases between the StrN-OccN ($p < 0.025$) and MRN-PAN ($p < 0.05$). Once again, these differences were not found in the control group (Cohort 2), which showed no significant differences in partialized connectivity between the two time points spaced by 1 month, but for a small but significant increase in the StrN–SCN coupling (Fig. 4). Consistent with an increase in global FC (Fig. 2) not matched by a comparable increase in direct interactions, the indirect FC was also increased by alcohol drinking (two-tailed Wilcoxon matched-pairs signed-rank test, $p < 0.0001$; Fig. 3*C*). Particularly important was the increase among the MRN, SCN, and PAN networks, suggesting a functional clustering driven by alcohol consumption.

These analyses demonstrated that 1 month of alcohol drinking induces a global increase in functional coupling between RSNs, mainly explained by an increase in global versus specific interactions, thus increasing the redundancy of the information shared in the network. Importantly though, the analysis further showed a redistribution in the equilibrium of functional connections, resulting in a change in the proportion of specific pairwise interactions between defined RSNs. It has been suggested, however, that when the number of observations per network node is limited, as often occurs in fMRI experiments, an efficient method to estimate the complete set of direct interactions is to compute a partial correlation with a Lasso regularization (Smith et al., 2011). Therefore, we next set out to validate our findings with L2 regularized partial correlation computed at the two time points, TP1 and TP2, in water-drinking controls and alcohol-exposed animals, and testing the differences (TP2 – TP1) between both groups. We found strong statistical interaction between RSNs and group (two-way ANOVAL $F_{(20,714)} = 5.9$, $p < 0.0001$). *Post hoc* Bonferroni's multiple-comparisons test identified a significant decrease in connectivity between the StrN and OccN ($t_{(714)} = 3.1$, $p = 0.046$), and increased connectivity between the StrN and mPCN ($t_{(714)} = 7.1$, $p < 0.0001$) and the PAN and SCN ($t_{(714)} = 3.2$, $p = 0.03$; Fig. 5). These results support the findings using multivariate regression models.

We next investigated whether the FC alterations persisted or recovered after the cessation of alcohol drinking. In a group of animals, we interrupted the access to alcohol for 1 week, acquiring a new imaging dataset after this period and computing full, partial, and indirect relations in the network of RSNs (Fig. 6). We found no statistically significant differences in the abstinence condition versus alcohol drinking. Similarly, L2 regularized partial correlation between RSNs during early abstinence showed no significant differences with respect to the alcohol-drinking condition (all corrected p-values > 0.05). However, since these analyses were performed in a subgroup of animals, the reduction in the sample size in the abstinence group has to be considered when interpreting this result. Overall, these results suggest the idea of an alcohol-driven reorganization of between-networks FC that sets a new equilibrium of specific interactions that persists in the initial stage of abstinence.

Brain activity measured by MEMRI is increased by alcohol drinking in awake rats

To directly assess regional brain activity in awake rats, we used two different protocols of MEMRI. In the first protocol, $MnCl_2$ was administered within a time window of 7 d using osmotic minipumps and produced no detectable effects on the behavior of the animal, including motor activity, and did not interfere with the amount of daily alcohol intake (4.4 ± 0.6 vs 4.4 ± 0.5 g/kg/d in the 7 d before vs after $MnCl_2$ infusion, respectively; two-tailed paired t test, $t_{(13)} = 0.21$ $p > 0.05$), as previously shown

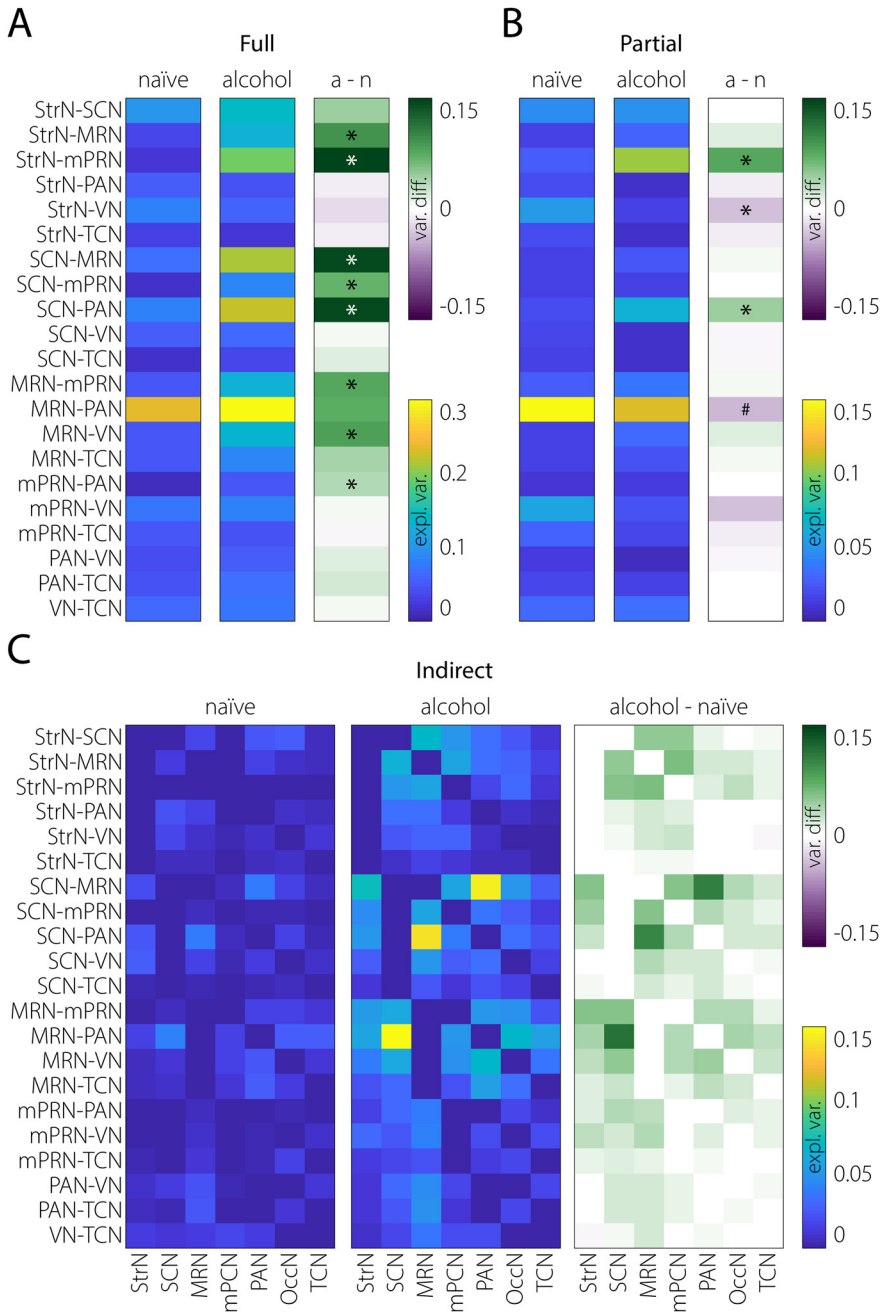

Figure 3. An increase in global connectivity alters the balance of functional weights among RSNs. ***A***, Full interactions in the network computed as the total variance of each link that can be explained by the activity in all the other nodes (6 links per node, 7 nodes or RSNs, 21 links in total). The explained variance (var.) for the naive (n) and alcohol (a) conditions is color coded (blue-to-yellow), as is the difference (diff.) between both conditions (a − n; red-to-green). ***B***, Same as ***A*** but for direct interactions, showing the specific (partialized) information shared by two RSNs that cannot be explained by any other RSN. ***C***, Same as ***A*** and ***B*** but for indirect interactions, representing the information between two RSNs (indicated on the *y*-axis) that is mediated by a third RSN (indicated on the *x*-axis). #$p < 0.05$, *$p < 0.025$.

(Eschenko et al., 2010a,b; Dudek et al., 2015, 2016; Pallarés et al., 2021). In the second protocol, the same dose of $MnCl_2$ (80 mg/kg, i.p.), administered acutely, produced an observable decrease in motor activity (Eschenko et al., 2010a,b) and a 31.5% reduction in alcohol intake (from 4.6 ± 0.7 to 2.8 ± 0.7 g/kg) over the 24 h post-$MnCl_2$ administration period (two-tailed paired *t* test, $t_{(7)} = 2.61$ $p = 0.04$). Daily consumption in the three groups exposed to alcohol, the rs-fMRI Cohort 1 and the two MEMRI experiments (before $MnCl_2$ administration), was undistinguishable (ANOVA: $F_{(2,37)} = 0.47$, $p = 0.63$).

Importantly, both manganese regime administrations produced comparable results. Statistical parametric maps for both MEMRI experiments are presented in Figure 7 and demonstrate significant (cluster size corrected, $p < 0.05$) increases of T1 signal intensity in the alcohol-drinking rats compared with the control conditions. More conservative cluster-size corrections yielded no statistically significant results. However, the replication of the MEMRI results in two independent experiments, and with brain-wide statistics, demonstrated the robustness of the findings. Additional experiments increasing the $MnCl_2$ administration dose to increase the signal-to-noise ratio were not considered because of the associated toxic effects (see above). No decreases in T1 signal were found to be statistically significant. An increase in T1 intensity reflects the accumulation of Mn^{2+} into brain tissue and suggests increased brain activation (Fig. 7). Activity increases were largely confined to prefrontal cortical regions, mostly the orbitofrontal, anterior insular, prelimbic, and infralimbic regions, and cingulate cortices (corresponding to the mPCN in rs-fMRI). Less extensive but significant activations were also found in primary and secondary motor regions and retrosplenial cortex (MRN) and S1 (SCN). Subcortically, the caudate–putamen and ventral striatum (StrN) showed statistically significant signal increases. Olfactory areas such as the olfactory bulb, anterior olfactory nucleus, and piriform cortex were also identified. The time course of the MEMRI experiment with acute manganese administration better matched the time course of the fMRI experiment, in which FC is measured in the last 24 h of alcohol drinking but had behavioral side effects. On the other hand, the administration with osmotic minipumps results in the integration of activity over the last 7 d of the alcohol-drinking period but did not interfere with the behavior of the animals. Both together, yielding highly comparable activation maps, produced a robust result showing activations in four of seven RSNs, with the strongest activations found in the mPCN followed by StrN and MRN (Fig. 7*D*). Neuronal activity as measured by MEMRI did not provide evidence in support of brain regions downregulating their activity after 1 month of chronic alcohol drinking.

Discussion

We show that a relatively brief period of chronic excessive alcohol drinking is enough to induce alterations in rs-fMRI

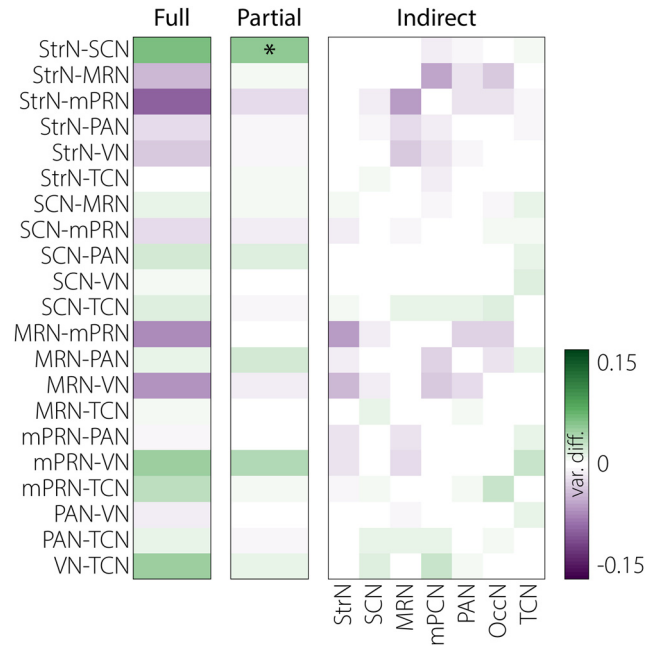

Figure 4. Global, direct, and indirect interactions among the water-drinking controls over 1 month. Animals in Cohort 2 were scanned at two TPs in naive conditions within a 30 d interval. Shown are the differences (TP2 − TP1) in full, direct, and indirect network interactions, color coded as in Figure 3. *$p < 0.025$.

connectivity and MEMRI brain activity. These alterations were age independent and supported by findings both in anesthetized and awake conditions, respectively. By combining both imaging techniques, we show a convergent increase in activity and altered connectivity in prefrontal cortical and ventral striatal structures. In the cortex, the AI, prelimbic, infralimbic, and cingulate cortices accumulate the strongest evidence of alteration driven by alcohol drinking. Quantifying the longitudinal transformations from an alcohol-naive state to a chronic drinking situation, we highlight two important adaptations. First, there is an early increase in redundant activity shared by all RSNs that decreases the specific information content in the system. We called this effect network dedifferentiation, as the activity becomes more similar across all network nodes. Second, the increase in correlated activity is heterogeneous, causing the rearrangement of pair-wise interactions. Reminiscent of a system that finds its equilibrium away from the original homeostatic state, the new highly correlated equilibrium allocates specific interactions between pairs of RSNs differently. We called this effect network narrowing, since the new equilibrium preserves most of the pair-wise interactions but retunes a specific set of connections, potentiating some and depressing others. These alterations persisted after drinking cessation, further suggesting an alcohol-induced allostatic load in the brain (Koob and Moal, 1997; Koob, 2003; McEwen, 2019) that does not recover during the first week of alcohol withdrawal.

The strength and novelty of our findings rely on the following three fundamental aspects of the study design: (1) the use of an animal model with demonstrated translational validity (Ciccocioppo et al., 2006; Hansson et al., 2006; Hirth et al., 2016; De Santis et al., 2019, 2020); (2) the use of two convergent imaging modalities that reinforce each other and allow the investigation of neuronal activity and connectivity, noninvasively and in the entire brain; and (3) the within-subject longitudinal design, possible in animal models, which is optimal for identifying the transformations during the trajectory from a naive state to a chronic alcohol-drinking state. In human studies, cross-sectional designs are the standard, with the control group used to contrast brain changes in AUD patients commonly composed by social drinkers. Furthermore, by using the animal model we avoid the comorbidities and heterogeneous drinking habits normally associated with AUD patients, allowing causal inference on the effects of alcohol.

Brain functional connectivity

The RSNs found in our work are consistent with those found in other rodent fMRI studies (Hutchison et al., 2010; Becerra et al., 2011; Lu et al., 2012; Tsai et al., 2020) and are common to RSNs found in humans (Smith et al., 2009). The first observation was a predominant, although heterogeneous, increase in the interactions among all RSNs at an early stage of chronic alcohol drinking. This observation, together with the increase in brain activation found with MEMRI, points to an initial hyperactive and hyperconnected state induced early by chronic alcohol drinking. These results resonate with some rs-fMRI findings in long-term AUD patients (Zhu et al., 2017) and contrast with others (Vergara et al., 2017). However, finding a translational counterpart for our observations in the literature might be difficult because they were obtained from a longitudinal experiment, which is not feasible in AUD patients, and were focused on brain-wide interactions in an early stage of chronic alcohol drinking, which is not commonly investigated in clinal studies. Therefore, this initial hyperactive and hyperconnected state might have been overlooked in clinical studies. Supporting this view, a study in alcohol-dependent and abstinent mice using the expression of the immediate early gene c-*fos* as a readout of neuronal activity, found widespread increases in correlated activation producing a decrease in brain network modularity (Kimbrough et al., 2020). Decreased modularity can be equated here with network dedifferentiation, which translates into less compartmentalized communication channels. Furthermore, as mentioned before, clinical studies suffer from various potential confounds, including somatic and psychiatric comorbidities and different patterns of abuse, likely contributing to the large variability of the results found in fMRI studies. For instance, a study with 188 subjects (including drinking, smoking, and drinking-and-smoking subjects) that found network alterations suggesting network hypoconnectivity, also showed that the concurrent use of nicotine and alcohol affects brain connectivity, requiring careful consideration of interaction effects (Vergara et al., 2017). Another recent study investigating network interactions globally in AUD patients, rather than seed-based studies or studies with a priori selection of ROI, has shown network alterations consistent with hyperconnectivity, with participation of the salience, default mode, executive, and reward networks (Zhu et al., 2017). Overall, these results highlight the importance of translational studies involving well controlled animal models to establish causal relations and investigate underlying mechanisms in AUD.

For the pair-wise alcohol-induced and abstinence-persistent changes in FC identified in our study, we can also find translational counterparts in separate human studies. The increase in the specific interaction between mPCN and StrN confirms the finding of increased resting-state FC between the anterior cingulate cortex and the striatum found in a seed-based analysis in 27 abstinent alcoholic subjects (16 ± 12.8 weeks of abstinence) versus 26 age-matched control subjects (Müller-Oehring et al., 2015). Similarly, the shift in maximal FC strength of the

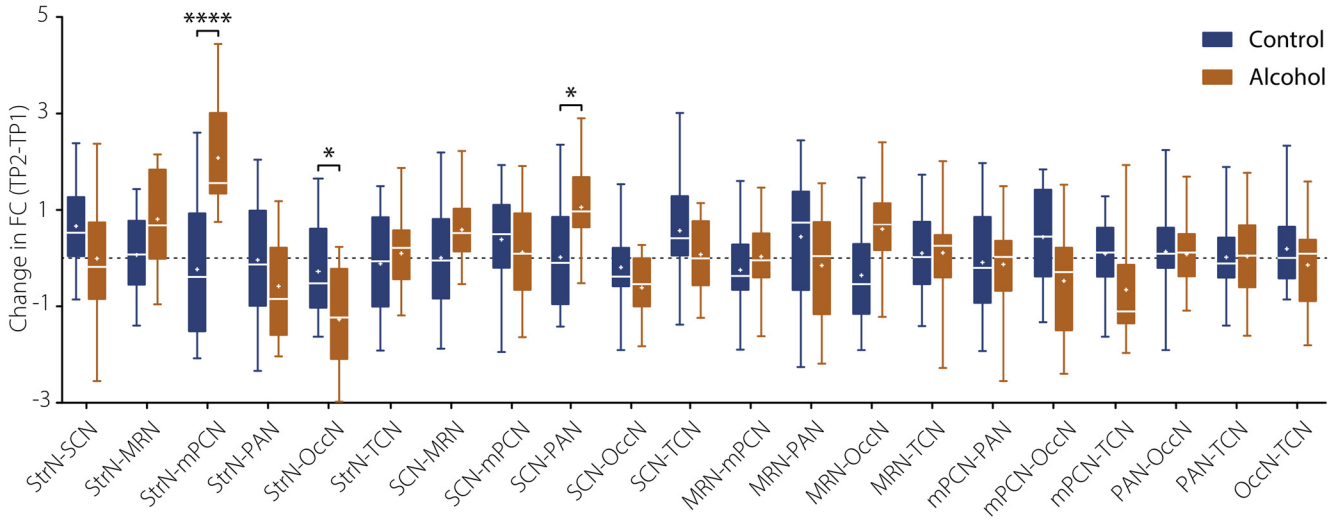

Figure 5. Specific interactions between RSN pairs are rebalanced by alcohol drinking. Alcohol induced both reductions and increments of partial correlation. The boxplots show the difference in partial correlation (L2-regularized, *pcorr* Fisher's *z* values) for all pairs of RSNs. The central mark of the box indicates the median, and the bottom and top edges of the box indicate the 25th and 75th percentiles, respectively. The whiskers extend to the most extreme data points. ****$p < 0.0001$, *$p < 0.05$.

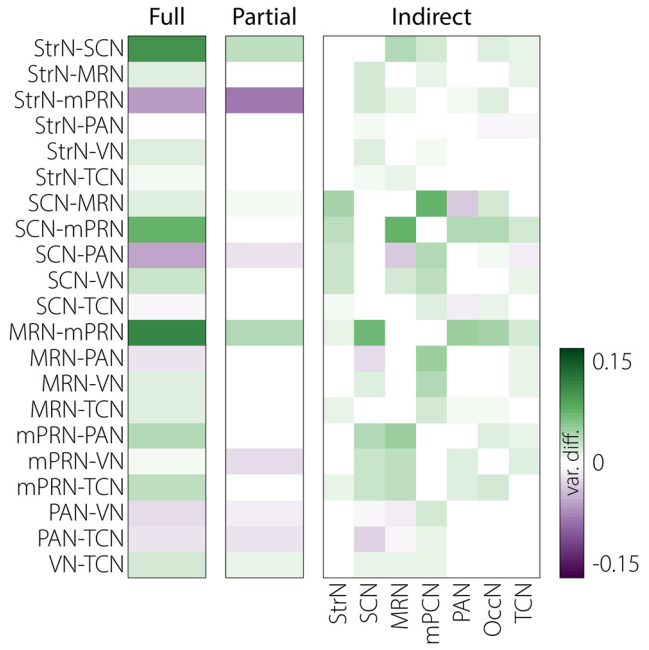

Figure 6. Differences in global, direct, and indirect interactions between the alcohol condition and early abstinence. After 1 month of voluntary alcohol consumption, alcohol was removed and a new MRI session was performed after 1 week of abstinence. Shown are the differences (abstinence – alcohol) in full, direct, and indirect network interactions, color coded as in Figure 3. No statistically significant differences were found.

orbitofrontal cortex toward the ventral striatum, was found in another resting-state study comparing 66 AUD patients with 40 healthy control subjects (Gerchen et al., 2019). Peak strength connectivity in this study correlated with alcohol dependency and the urge to consume alcohol. Using between-RSNs connectivity as features in a machine learning platform, a recent study showed that pair-wise connectivity between the reward network (largely involving our StrN) and the executive control and default mode networks (with key structures represented in the mPCN) conveyed the maximal information to classify AUD patients ($n = 46$ vs 46 healthy control subjects; Zhu et al., 2018). Finally, the anterior insular cortex, an important region of the salience network and contained in our mPCN, was highlighted in several AUD fMRI studies, with a postulated role in the dysregulation of interoceptive awareness in drinkers (Orban et al., 2013; Vergara et al., 2017; Zhu et al., 2017; Halcomb et al., 2019; Bordier et al., 2022; for review, see Sommer et al., 2022). Strengthened connectivity within an amygdalar–striatal network, compatible with the increased mPCN–StrN-specific interaction, was found in a cohort of 25 alcohol-dependent patients and 26 healthy control subjects, with a salience network correlating with impulsivity measured in the delay discount task (Zhu et al., 2017).

The decrease in FC between OccN and SCN matches the visuomotor hypoconnectivity found in social drinkers after acute alcohol consumption (Luchtmann et al., 2013) and, in AUD patients, connectivity between the occipital gyrus and the supplementary motor area negatively correlated with AUDIT (Alcohol Use Disorders Identification Test) values (Fede et al., 2019). The finding in social drinkers confirmed that the visuomotor pathway is affected early during alcohol drinking, and further indicated that alterations in these networks may persist even during early abstinence. Furthermore, a recent study in a cohort of adults with problem drinking patterns ($n = 59$) showed that connectivity with visual, visual association, and sensorimotor regions was important for predicting AUD severity (Fede et al., 2019). Another rs-fMRI study with 43 volunteers diagnosed with AUD and 26 healthy control subjects using the striatum as the seed region (Kohno et al., 2017) found increased FC with the anterior cingulate cortex in the AUD group and decreased connectivity with the lateral occipital cortex, equivalent to the increased StrN–mPCN and decreased StrN–OccN connectivity, respectively, found in our present study. These studies pointed to relapse vulnerability because of craving dysregulation reflected in the increased connectivity in striatolimbic regions and decreased corticostriatal connectivity. Our preclinical study supports this interpretation and further indicates that these changes can be directly linked to alcohol, starting soon after chronic excessive drinking begins, and propagate into early abstinence.

Brain activity

MEMRI allowed us to assess the effects of chronic alcohol consumption on global brain activity in freely behaving animals.

MEMRI activations were mostly localized in the striatum and prefrontocortical structures. Activity in the ventral striatum occurs during reinforced learning and has long been associated with the rewarding effects of drugs of abuse, including alcohol (Koob et al., 1998). Comparable evidence supporting the striatal activation in different rat models of alcohol consumption have been reported using 2-deoxyglucose uptake (Porrino et al., 1998) or c-Fos immunostaining (Bachtell et al., 1999; Hansson et al., 2007; Vilpoux et al., 2009), and alcohol consumption was shown to evoke dopamine release in the accumbens of sP rats, the parental strain of msPs (De Montis et al., 2004). In humans, ventral striatal activation has been consistently found to be associated with the presentation of alcoholic beverages or related sensory cues (Myrick et al., 2004; Filbey et al., 2008; Gilman et al., 2008; Vollstädt-Klein et al., 2020).

Brain regions in the basic motivational circuit have also been consistently found in imaging studies with AUD patients, including medial and orbital regions of the prefrontal cortex (Spanagel, 2009) and insular cortex (Naqvi and Bechara, 2010), which were also found in our MEMRI maps. Activation of the insular cortex and ventral striatum in response to alcohol cues further correlated with drinking levels in humans (Ihssen et al., 2011). Activations in both the prelimbic and infralimbic subdivisions of the medial prefrontal cortex were found in a postdependent rat model of alcohol addiction (Meinhardt and Sommer, 2015), likely associated with the alcohol-dependent phenotype. It is important to note that both structures are part of the mPCN identified in our rs-fMRI study, which showed enhanced direct interaction with the StrN; that is, both structures and the NAc are more active (MEMRI) and functionally coupled (rs-fMRI) after chronic alcohol drinking, with a likely effect on the reward system (Haber and Knutson, 2010). In msP rats, with an innate anxiety-like behavior (Ciccocioppo et al., 2006; Borruto et al., 2021), the infralimbic connection may contribute to the anxiolytic effects of alcohol, whereas the medial prefrontal cortex activation could mediate alcohol-seeking behavior (Peters et al., 2009; Meinhardt et al., 2013; Pfarr et al., 2015, 2018). We have previously hypothesized that msP rats are a phenocopy of a postdependent alcohol condition in which alcohol is consumed as an attempt to self-medicate from high background levels of stress (Hansson et al., 2006; Björk et al., 2010; Herman et al., 2013; Hirth et al., 2016). In this context, the combined rs-fMRI and MEMRI results may be interpreted as an allostatic network reorganization induced by alcohol to compensate a preexisting dysfunction that leads to the chronification of alcohol consumption.

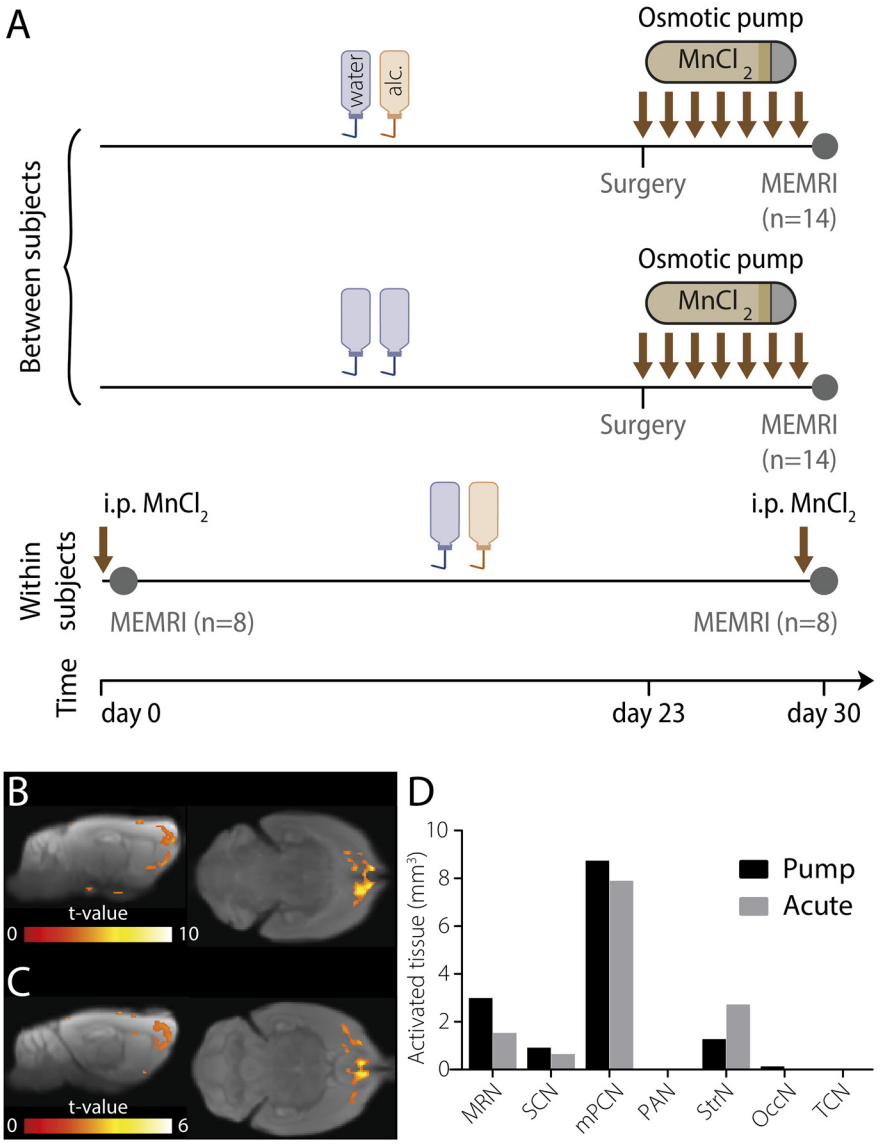

Figure 7. One month of alcohol drinking in msP rats increased brain activity in frontal and striatal regions. ***A***, Scheme of the MEMRI experiments with cross-sectional design (between subjects, two groups of $n = 14$ each) and longitudinal design (within subjects, one group of $n = 8$). For details, see Materials and Methods. ***B***, Two representative slices (sagittal and horizontal) of the MEMRI maps in the cross-sectional study using osmotic minipumps to deliver $MnCl_2$. Maps represent statistically significant differences (alcohol > control, colors indicating t values) after cluster-size correction (corrected $p < 0.05$). ***C***, Same as ***B*** but for the longitudinal study using acute intraperitoneal injection to deliver the same dose of $MnCl_2$. ***D***, Volume of tissue showing increased MEMRI signal in ethanol drinking versus naive animals at the statistical threshold ($p < 0.05$) shown in ***B*** and ***C*** in different brain regions corresponding to the RSNs defined in the fMRI study.

Study limitations

Some limitations of the present study need to be considered. First, for the reasons stated in the introduction, fMRI experiments in awake rat AUD models present important drawbacks, and, thus, the RSN activity was extracted from lightly anesthetized animals. While previous studies showed robust RSNs in anesthetized versus awake conditions (Barttfeld et al., 2015; Díaz-Parra et al., 2017; Paasonen et al., 2018), important network dynamics could have been masked. This limitation was avoided in the MEMRI study, in which manganese accumulation occurs in awake animals, although it reflects neuronal activity rather

than connectivity. On the other hand, the sensitivity of the MEMRI technique to map brain activity relies on manganese ion concentration in the extracellular space, but increasing it over certain limits may result in toxic effects (Eschenko et al., 2010a, b). To overcome this limitation and the trade-off of sensitivity and toxicity, we used low doses of $MnCl_2$ and two different regimes of administration, as previously described (Eschenko et al., 2010a). The obtained results were highly robust across protocols. However, subtler alterations in brain activity may have gone undetected by these protocols. An important consideration is also the complexity of AUD, resulting from several genetic, environmental, and personality factors, and therefore is hardly represented by a single animal model. The msP line, in addition to showing a preference for alcohol, presents high stress sensitivity and a propensity to negative affect (Borruto et al., 2021), and therefore, it more likely resembles a subpopulation of AUD patients that drink to alleviate negative mood and for stress-relieving purposes. More generally, the 1 month period of drinking in rats is not expected to mimic all the effects of alcohol consumption in long-term AUD patients, but more likely the early transformations induced by chronic drinking. The translational validity of the model, however, has been validated in several recent studies (De Santis et al., 2019, 2020). Finally, the present study was performed in males. However, important sex differences in alcohol exposure have been found (Agabio et al., 2017; Fama, 2020) that warrant further work comparing RSN connectivity and brain activity in males and females.

Concluding remarks

To conclude, we combined rs-fMRI and MEMRI in msP rats engaged in chronic moderate drinking, to investigate brain adaptations induced by alcohol drinking and withdrawal. Alcohol drinking led to a global but heterogeneous increase in BOLD signal correlation and a concomitant increase in activity in frontal and prefrontal cortical regions and striatal areas. This new network configuration relays communication through indirect pathways, favoring global over local information processing. We hypothesize that increased neuronal excitability is responsible for both enhanced neuronal activation and functional coupling in RSNs. We further hypothesize that the increased redundancy in network interactions (dedifferentiation) produced by the alcohol-driven hyperconnected state compromises cognitive function. Because of its heterogeneous nature, the global increase in FC produces a second brain adaptation that involves the readjustment of a specific set of connections between pairs of RSNs, remodeling specific pathways and narrowing communication channels. Importantly, these alterations persisted after alcohol discontinuation, during abstinence, suggesting that the brain network reaches a new functional equilibrium after a relatively brief period of chronic alcohol consumption that does not recover spontaneously, at least during the early stage of abstinence. Whether this new state contributes to the vulnerability to relapse needs to be investigated. Initial studies involving chemogenetic manipulation of distinct network nodes (Haaranen et al., 2020) suggest that those manipulations involve highly complex networks and that their behavioral outcomes are difficult to predict. Future research using animal models is needed to understand this transition to develop therapies aiming to recover the network homeostasis.

References

Agabio R, Pisanu C, Gessa GL, Franconi F (2017) Sex differences in alcohol use disorder. Curr Med Chem 24:2661–2670.

Bachtell RK, Wang YM, Freeman P, Risinger FO, Ryabinin AE (1999) Alcohol drinking produces brain region-selective changes in expression of inducible transcription factors. Brain Res 847:157–165.

Bangasser DA, Lee CS, Cook PA, Gee JC, Bhatnagar S, Valentino RJ (2013) Manganese-enhanced magnetic resonance imaging (MEMRI) reveals brain circuitry involved in responding to an acute novel stress in rats with a history of repeated social stress. Physiol Behav 122:228–236.

Barttfeld P, Uhrig L, Sitt JD, Sigman M, Jarraya B, Dehaene S (2015) Signature of consciousness in the dynamics of resting-state brain activity. Proc Natl Acad Sci U|S|A 112:887–892.

Becerra L, Pendse G, Chang PC, Bishop J, Borsook D (2011) Robust reproducible resting state networks in the awake rodent brain. PLoS One 6: e25701.

Beckmann CF, Smith SM (2004) Probabilistic independent component analysis for functional magnetic resonance imaging. IEEE Trans Med Imaging 23:137–152.

Beckmann CF, DeLuca M, Devlin JT, Smith SM (2005) Investigations into resting-state connectivity using independent component analysis. Philos Trans R Soc Lond B Biol Sci 360:1001–1013.

Beckmann CF, Mackay CE, Filippini N, Smith SM (2009) Group comparison of resting-state FMRI data using multi-subject ICA and dual regression. Neuroimage 47 [Suppl 1]:S148.

Björk K, Hansson AC, Sommer WH (2010) Genetic variation and brain gene expression in rodent models of alcoholism. Int Rev Neurobiol 91:129–171.

Bordier C, Weil G, Bach P, Scuppa G, Nicolini C, Forcellini G, Pérez-Ramirez U, Moratal D, Canals S, Hoffmann S, Hermann D, Vollstädt-Klein S, Kiefer F, Kirsch P, Sommer WH, Bifone A (2022) Increased network centrality of the anterior insula in early abstinence from alcohol. Addict Biol 27:e13096.

Borruto AM, Stopponi S, Li H, Weiss F, Roberto M, Ciccocioppo R (2021) Genetically selected alcohol-preferring msP rats to study alcohol use disorder: anything lost in translation? Neuropharmacology 186:108446.

Cannella N, Cosa-Linan A, Takahashi T, Weber-Fahr W, Spanagel R (2020) Cocaine addicted rats show reduced neural activity as revealed by manganese-enhanced MRI. Sci Rep 10:19353.

Chanraud S, Pitel AL, Pfefferbaum A, Sullivan EV (2011) Disruption of functional connectivity of the default-mode network in alcoholism. Cereb Cortex 21:2272–2281.

Ciccocioppo R (2013) Genetically selected alcohol preferring rats to model human alcoholism. Curr Top Behav Neurosci 13:251–269.

Ciccocioppo R, Economidou D, Cippitelli A, Cucculelli M, Ubaldi M, Soverchia L, Lourdusamy A, Massi M (2006) Genetically selected Marchigian Sardinian alcohol-preferring (msP) rats: an animal model to study the neurobiology of alcoholism. Addict Biol 11:339–355.

Cole DM, Smith SM, Beckmann CF (2010) Advances and pitfalls in the analysis and interpretation of resting-state FMRI data. Front Syst Neurosci 4:8.

De Montis MG, Grappi S, Gambarana C, Leggio B, Nanni G, Scheggi S, Tagliamonte A (2004) Sardinian alcohol-preferring rats show low 5-HT extraneuronal levels in the mPFC and no habituation in monoaminergic response to repeated ethanol consumption in the NAcS. Brain Res 1006:18–27.

De Santis S, Sommer WH, Canals S (2019) Detecting alcohol-induced brain damage noninvasively using diffusion tensor imaging. ACS Chem Neurosci 10:4187–4189.

De Santis S, Cosa-Linan A, Garcia-Hernandez R, Dmytrenko L, Vargova L, Vorisek I, Stopponi S, Bach P, Kirsch P, Kiefer F, Ciccocioppo R, Sykova E, Moratal D, Sommer WH, Canals S (2020) Chronic alcohol consumption alters extracellular space geometry and transmitter diffusion in the brain. Sci Adv 6:eaba0154.

Díaz-Parra A, Osborn Z, Canals S, Moratal D, Sporns O (2017) Structural and functional, empirical and modeled connectivity in the cerebral cortex of the rat. Neuroimage 159:170–184.

Dudek M, Abo-Ramadan U, Hermann D, Brown M, Canals S, Sommer WH, Hyytiä P (2015) Brain activation induced by voluntary alcohol and saccharin drinking in rats assessed with manganese-enhanced magnetic resonance imaging. Addict Biol 20:1012–1021.

Dudek M, Canals S, Sommer WH, Hyytiä P (2016) Modulation of nucleus accumbens connectivity by alcohol drinking and naltrexone in alcohol-preferring rats: a manganese-enhanced magnetic resonance imaging study. Eur Neuropsychopharmacol 26:445–455.

Dupuy M, Chanraud S (2016) Imaging the addicted brain: alcohol. Int Rev Neurobiol 129:1–31.
Eschenko O, Canals S, Simanova I, Beyerlein M, Murayama Y, Logothetis NK (2010a) Mapping of functional brain activity in freely behaving rats during voluntary running using manganese-enhanced MRI: implication for longitudinal studies. Neuroimage 49:2544–2555.
Eschenko O, Canals S, Simanova I, Logothetis NK (2010b) Behavioral, electrophysiological and histopathological consequences of systemic manganese administration in MEMRI. Magn Reson Imaging 28:1165–1174.
Fama R (2020) Alcohol's unique effects on cognition in women. Alcohol Res 40:03.
Fede SJ, Grodin EN, Dean SF, Diazgranados N, Momenan R (2019) Resting state connectivity best predicts alcohol use severity in moderate to heavy alcohol users. NeuroImage Clin 22:101782.
Filbey FM, Claus E, Audette AR, Niculescu M, Banich MT, Tanabe J, Du YP, Hutchison KE (2008) Exposure to the taste of alcohol elicits activation of the mesocorticolimbic neurocircuitry. Neuropsychopharmacology 33:1391–1401.
Fox MD, Raichle ME (2007) Spontaneous fluctuations in brain activity observed with functional magnetic resonance imaging. Nat Rev Neurosci 8:700–711.
Friston KJ, Holmes AP, Worsley KJ, Poline J-P, Frith CD, Frackowiak RSJ (1994) Statistical parametric maps in functional imaging: a general linear approach. Hum Brain Mapp 2:189–210.
Gerchen MF, Rentsch A, Kirsch M, Kiefer F, Kirsch P (2019) Shifts in the functional topography of frontal cortex-striatum connectivity in alcohol use disorder. Addict Biol 24:1245–1253.
Gildish I, Manor D, David O, Sharma V, Williams D, Agarwala U, Wang X, Kenney JW, Proud CG, Rosenblum K (2012) Impaired associative taste learning and abnormal brain activation in kinase-defective eEF2K mice. Learn Mem 19:116–125.
Gilman JM, Ramchandani VA, Davis MB, Bjork JM, Hommer DW (2008) Why we like to drink: a functional magnetic resonance imaging study of the rewarding and anxiolytic effects of alcohol. J Neurosci 28:4583–4591.
Griffanti L, Salimi-Khorshidi G, Beckmann CF, Auerbach EJ, Douaud G, Sexton CE, Zsoldos E, Ebmeier KP, Filippini N, Mackay CE, Moeller S, Xu J, Yacoub E, Baselli G, Ugurbil K, Miller KL, Smith SM (2014) ICA-based artefact removal and accelerated fMRI acquisition for improved resting state network imaging. Neuroimage 95:232–247.
Haaranen M, Scuppa G, Tambalo S, Järvi V, Bertozzi SM, Armirotti A, Sommer WH, Bifone A, Hyytiä P (2020) Anterior insula stimulation suppresses appetitive behavior while inducing forebrain activation in alcohol-preferring rats. Transl Psychiatry 10:150.
Haber SN, Knutson B (2010) The reward circuit: linking primate anatomy and human imaging. Neuropsychopharmacology 35:4–26.
Halcomb ME, Chumin EJ, Goñi J, Dzemidzic M, Yoder KK (2019) Aberrations of anterior insular cortex functional connectivity in non-treatment-seeking alcoholics. Psychiatry Res Neuroimaging 284:21–28.
Hansson AC, Cippitelli A, Sommer WH, Fedeli A, Björk K, Soverchia L, Terasmaa A, Massi M, Heilig M, Ciccocioppo R (2006) Variation at the rat Crhr1 locus and sensitivity to relapse into alcohol seeking induced by environmental stress. Proc Natl Acad Sci U|S|A 103:15236–15241.
Hansson AC, Cippitelli A, Sommer WH, Ciccocioppo R, Heilig M (2007) Region-specific down-regulation of Crhr1 gene expression in alcohol-preferring msP rats following ad lib access to alcohol. Addict Biol 12:30–34.
Heilig M, Augier E, Pfarr S, Sommer WH (2019) Developing neuroscience-based treatments for alcohol addiction: a matter of choice? Transl Psychiatry 9:255.
Herman MA, Contet C, Justice NJ, Vale W, Roberto M (2013) Novel subunit-specific tonic GABA currents and differential effects of ethanol in the central amygdala of CRF receptor-1 reporter mice. J Neurosci 33:3284–3298.
Hirth N, Meinhardt MW, Noori HR, Salgado H, Torres-Ramirez O, Uhrig S, Broccoli L, Vengeliene V, Roßmanith M, Perreau-Lenz S, Köhr G, Sommer WH, Spanagel R, Hansson AC (2016) Convergent evidence from alcohol-dependent humans and rats for a hyperdopaminergic state in protracted abstinence. Proc Natl Acad Sci U|S|A 113:3024–3029.
Hutchison RM, Mirsattari SM, Jones CK, Gati JS, Leung LS (2010) Functional networks in the anesthetized rat brain revealed by independent component analysis of resting-state fMRI. J Neurophysiol 103:3398–3406.
Hyvärinen A (1997) A family of fixed-point algorithms for independent component analysis. In: 1997 international conference on acoustics, speech, and signal processing (ICASSP), Vol 5, pp 3917–3920. Los Alamitos, CA: IEEE Computer Society.
Ihssen N, Cox WM, Wiggett A, Fadardi JS, Linden DEJ (2011) Differentiating heavy from light drinkers by neural responses to visual alcohol cues and other motivational stimuli. Cereb Cortex 21:1408–1415.
Jenkinson M, Bannister P, Brady M, Smith S (2002) Improved optimization for the robust and accurate linear registration and motion correction of brain images. Neuroimage 17:825–841.
Jenkinson M, Beckmann CF, Behrens TE, Woolrich MW, Smith SM (2012) Neuroimage 62:782–790.
Kalthoff D, Seehafer JU, Po C, Wiedermann D, Hoehn M (2011) Functional connectivity in the rat at 11.7 T: impact of physiological noise in resting state fMRI. Neuroimage 54:2828–2839.
Kimbrough A, Lurie DJ, Collazo A, Kreifeldt M, Sidhu H, Macedo GC, D'Esposito M, Contet C, George O (2020) Brain-wide functional architecture remodeling by alcohol dependence and abstinence. Proc Natl Acad Sci U|S|A 117:2149–2159.
Kohno M, Dennis LE, McCready H, Hoffman WF (2017) Executive control and striatal resting-state network interact with risk factors to influence treatment outcomes in alcohol-use disorder. Front Psychiatry 8:182.
Koob GF (2003) Alcoholism: allostasis and beyond. Alcohol Clin Exp Res 27:232–243.
Koob GF, Moal ML (1997) Drug abuse: hedonic homeostatic dysregulation. Science 278:52–58.
Koob GF, Roberts AJ, Schulteis G, Parsons LH, Heyser CJ, Hyytiä P, Merlo-Pich E, Weiss F (1998) Neurocircuitry targets in ethanol reward and dependence. Alcohol Clin Exp Res 22:3–9.
Laine MA, Sokolowska E, Dudek M, Callan S-A, Hyytiä P, Hovatta I (2017) Brain activation induced by chronic psychosocial stress in mice. Sci Rep 7:15061.
López-Madrona VJ, Pérez-Montoyo E, Álvarez-Salvado E, Moratal D, Herreras O, Pereda E, Mirasso CR, Canals S (2020) Different theta frameworks coexist in the rat hippocampus and are coordinated during memory-guided and novelty tasks. Elife 9:e57313.
Lu H, Zou Q, Gu H, Raichle ME, Stein EA, Yang Y (2012) Rat brains also have a default mode network. Proc Natl Acad Sci U|S|A 109:3979–3984.
Luchtmann M, Jachau K, Adolf D, Baecke S, Lützkendorf R, Müller C, Tempelmann C, Bernarding J (2013) Decreased effective connectivity in the visuomotor system after alcohol consumption. Alcohol 47:195–202.
McEwen BS (2019) The good side of "stress". Stress 22:524–525.
McGuire JL, Bergstrom HC, Parker CC, Le T, Morgan M, Tang H, Selwyn RG, Silva AC, Choi K, Ursano RJ, Palmer AA, Johnson LR (2013) Traits of fear resistance and susceptibility in an advanced intercross line. Eur J Neurosci 38:3314–3324.
Meinhardt MW, Sommer WH (2015) Postdependent state in rats as a model for medication development in alcoholism. Addict Biol 20:1–21.
Meinhardt MW, Hansson AC, Perreau-Lenz S, Bauder-Wenz C, Stählin O, Heilig M, Harper C, Drescher KU, Spanagel R, Sommer WH (2013) Rescue of infralimbic mGluR2 deficit restores control over drug-seeking behavior in alcohol dependence. J Neurosci 33:2794–2806.
Moreno A, Jego P, de la Cruz F, Canals S (2013) Neurophysiological, metabolic and cellular compartments that drive neurovascular coupling and neuroimaging signals. Front Neuroenergetics 5:3.
Müller-Oehring EM, Jung YC, Pfefferbaum A, Sullivan EV, Schulte T (2015) The resting brain of alcoholics. Cereb Cortex 25:4155–4168.
Myrick H, Anton RF, Li X, Henderson S, Drobes D, Voronin K, George MS (2004) Differential brain activity in alcoholics and social drinkers to alcohol cues: relationship to craving. Neuropsychopharmacology 29:393–402.
Naqvi NH, Bechara A (2010) The insula and drug addiction: an interoceptive view of pleasure, urges, and decision-making. Brain Struct Funct 214:435–450.
Orban C, McGonigle J, Kalk NJ, Erritzoe D, Waldman AD, Nutt DJ, Rabiner EA, Lingford-Hughes AR (2013) Resting state synchrony in anxiety-related circuits of abstinent alcohol-dependent patients. Am J Drug Alcohol Abuse 39:433–440.
Paasonen J, Stenroos P, Salo RA, Kiviniemi V, Gröhn O (2018) Functional connectivity under six anesthesia protocols and the awake condition in rat brain. Neuroimage 172:9–20.
Pacheco-Torres J, Moreno A, Fernández B, Pérez-Cervera L, Caramés JM, Fernández-Mollá LM, Pérez-Montoyo E, Moratal D, Canals S (2018)

Functional MRI of synaptic plasticity. In: Handbook of in vivo neural plasticity techniques: a systems neuroscience approach to the neural basis of memory and cognition, (Manahan-Vaughan D, ed), Vol 28, pp 441–456. London: Academic.

Pallarés V, Dudek M, Moreno A, Pérez-Ramírez Ú, Moratal D, Haaranen M, Ciccocioppo R, Sommer WH, Canals S, Hyytiä P (2021) Neuroimaging reveals functionally distinct neuronal networks associated with high-level alcohol consumption in two genetic rat models. Behav Pharmacol 32:229–238.

Pan WJ, Billings JC, Grooms JK, Shakil S, Keilholz SD (2015) Considerations for resting state functional MRI and functional connectivity studies in rodents. Front Neurosci 9:269.

Pan WJ, Thompson GJ, Magnuson ME, Jaeger D, Keilholz S (2013) Infraslow LFP correlates to resting-state fMRI BOLD signals. Neuroimage 74:288–297.

Paxinos G, Watson C (2007) The rat brain in stereotaxic coordinates, Ed 6. London: Academic.

Pérez-Cervera L, Caramés J, Fernández-Mollá L, Moreno A, Fernández B, Pérez-Montoyo E, Moratal D, Canals S, Pacheco-Torres J (2018) Mapping functional connectivity in the rodent brain using electric-stimulation fMRI. In: Methods in molecular biology, Ed 1 (García-Martín M, López-Larrubia P, eds), pp 117–134. Hatfield, UK: Humana.

Peters J, Kalivas PW, Quirk GJ (2009) Extinction circuits for fear and addiction overlap in prefrontal cortex. Learn Mem 16:279–288.

Pfarr S, Meinhardt MW, Klee ML, Hansson AC, Vengeliene V, Schönig K, Bartsch D, Hope BT, Spanagel R, Sommer WH (2015) Losing control: excessive alcohol seeking after selective inactivation of cue-responsive neurons in the infralimbic cortex. J Neurosci 35:10750–10761.

Pfarr S, Schaaf L, Reinert J, Paul E, Herrmannsdörfer F, Roßmanith M, Kuner T, Hansson A, Spanagel R, Körber C, Sommer W (2018) Choice for drug or natural reward engages largely overlapping neuronal ensembles in the infralimbic prefrontal cortex. J Neurosci 38:3507–3519.

Porrino LJ, Williams-Hemby L, Whitlow C, Bowen C, Samson HH (1998) Metabolic mapping of the effects of oral alcohol self-administration in rats. Alcohol Clin Exp Res 22:176–182.

Schwarz AJ, Danckaert A, Reese T, Gozzi A, Paxinos G, Watson C, Merlo-Pich EV, Bifone A (2006) A stereotaxic MRI template set for the rat brain with tissue class distribution maps and co-registered anatomical atlas: application to pharmacological MRI. Neuroimage 32:538–550.

Scuppa G, Tambalo S, Pfarr S, Sommer WH, Bifone A (2020) Aberrant insular cortex connectivity in abstinent alcohol-dependent rats is reversed by dopamine D3 receptor blockade. Addict Biol 25:e12744.

Silva AC, Lee JH, Aoki I, Koretsky AP (2004) Manganese-enhanced magnetic resonance imaging (MEMRI): methodological and practical considerations. NMR Biomed 17:532–543.

Smith DV, Utevsky AV, Bland AR, Clement N, Clithero JA, Harsch AE, McKell Carter R, Huettel SA (2014) Characterizing individual differences in functional connectivity using dual-regression and seed-based approaches. Neuroimage 95:1–12.

Smith SM (2002) Fast robust automated brain extraction. Hum Brain Mapp 17:143–155.

Smith SM, Brady JM (1997) SUSAN—a new approach to low level image processing. Int J Comput Vis 23:45–78.

Smith SM, Jenkinson M, Woolrich MW, Beckmann CF, Behrens TE, Johansen-Berg H, Bannister PR, De Luca M, Drobnjak I, Flitney DE, Niazy RK, Saunders J, Vickers J, Zhang Y, De Stefano N, Brady JM, Matthews PM (2004) Advances in functional and structural MR image analysis and implementation as FSL. Neuroimage 23:S208–S219.

Smith SM, Fox PT, Miller KL, Glahn DC, Fox PM, Mackay CE, Filippini N, Watkins KE, Toro R, Laird AR, Beckmann CF (2009) Correspondence of the brain's functional architecture during activation and rest. Proc Natl Acad Sci U|S|A 106:13040–13045.

Smith SM, Miller KL, Salimi-Khorshidi G, Webster M, Beckmann CF, Nichols TE, Ramsey JD, Woolrich MW (2011) Network modelling methods for FMRI. Neuroimage 54:875–891.

Smith SM, Nichols TE, Vidaurre D, Winkler AM, Behrens TE, Glasser MF, Ugurbil K, Barch DM, Van Essen DC, Miller KL (2015) A positive-negative mode of population covariation links brain connectivity, demographics and behavior. Nat Neurosci 18:1565–1567.

Sommer WH, Canals S, Bifone A, Heilig M, Hyytiä P (2022) From a systems view to spotting a hidden island: a narrative review implicating insula function in alcoholism. Neuropharmacology 209:108989.

Spanagel R (2009) Alcoholism: a systems approach from molecular physiology to addictive behavior. Physiol Rev 89:649–705.

Stenroos P, Paasonen J, Salo RA, Jokivarsi K, Shatillo A, Tanila H, Gröhn O (2018) Awake rat brain functional magnetic resonance imaging using standard radio frequency coils and a 3D printed restraint kit. Front Neurosci 12:548.

Topiwala A, Allan CL, Valkanova V, Zsoldos E, Filippini N, Sexton C, Mahmood A, Fooks P, Singh-Manoux A, Mackay CE, Kivimäki M, Ebmeier KP (2017) Moderate alcohol consumption as risk factor for adverse brain outcomes and cognitive decline: longitudinal cohort study. BMJ 357:j2353.

Tsai P-J, Keeley RJ, Carmack SA, Vendruscolo JCM, Lu H, Gu H, Vendruscolo LF, Koob GF, Lin C-P, Stein EA, Yang Y (2020) Converging structural and functional evidence for a rat salience network. Biol Psychiatry 88:867–878.

Vergara VM, Liu J, Claus ED, Hutchison K, Calhoun V (2017) Alterations of resting state functional network connectivity in the brain of nicotine and alcohol users. Neuroimage 151:45–54.

Vilpoux C, Warnault V, Pierrefiche O, Daoust M, Naassila M (2009) Ethanol-sensitive brain regions in rat and mouse: a cartographic review, using immediate early gene expression. Alcohol Clin Exp Res 33:945–969.

Vincent JL, Patel GH, Fox MD, Snyder AZ, Baker JT, Van Essen DC, Zempel JM, Snyder LH, Corbetta M, Raichle ME (2007) Intrinsic functional architecture in the anaesthetized monkey brain. Nature 447:83–86.

Vollstädt-Klein S, Mildner P, Bumb JM, Karl D, Ueberle C, Shevchenko Y, Kiefer F, Effelsberg W (2020) The training game SALIENCE for the therapy of alcohol use disorder. Health Informatics J 26:499–512.

Weiland BJ, Sabbineni A, Calhoun VD, Welsh RC, Bryan AD, Jung RE, Mayer AR, Hutchison KE (2014) Reduced left executive control network functional connectivity is associated with alcohol use disorders. Alcohol Clin Exp Res 38:2445–2453.

Winkler AM, Ridgway GR, Webster MA, Smith SM, Nichols TE (2014) Permutation inference for the general linear model. Neuroimage 92:381–397.

Winkler AM, Webster MA, Brooks JC, Tracey I, Smith SM, Nichols TE (2016) Non-parametric combination and related permutation tests for neuroimaging. Hum Brain Mapp 37:1486–1511.

World Health Organization (2018) Global status report on alcohol and health 2018 (Poznyak V, Rekve D, eds). Geneva: World Health Organization.

Yang J, Li Q (2020) Manganese-enhanced magnetic resonance imaging: application in central nervous system diseases. Front Neurol 11:143.

Zhang H, Wang S, Liu B, Ma Z, Yang M, Zhang Z, GJ T (2010) Resting brain connectivity: changes during the progress of Alzheimer disease. Radiology 256:598–606.

Zhu X, Sundby K, Bjork JM, Momenan R (2016) Alcohol dependence and altered engagement of brain networks in risky decisions. Front Hum Neurosci 10:142.

Zhu X, Cortes CR, Mathur K, Tomasi D, Momenan R (2017) Model-free functional connectivity and impulsivity correlates of alcohol dependence: a resting-state study. Addict Biol 22:206–217.

Zhu X, Du X, Kerich M, Lohoff FW, Momenan R (2018) Random forest based classification of alcohol dependence patients and healthy controls using resting state MRI. Neurosci Lett 676:27–33.